

Hazard Assessment Comparison of Tazhiping Landslide Before and After Treatment using the finite volume method

Dong Huang¹, YuanJun Jiang^{1*}, JianPing Qiao¹, Meng Wang¹

1. Key Laboratory of Mountain hazards and Surface process, Institute of Mountain hazards and Environment, Chinese Academy of Science, Chengdu 610041, China

*Corresponding author (yuanjun.jiang.civil@gmail.com).

Abstract: Through investigation and analysis of geological conditions and mechanical parameters of the Tazhiping landslide, the finite volume method was adopted, and, the rheological model was adopted to simulate the landslide and avalanche entire mass movement process. The present paper adopted the numerical approach of RAMMS and the GIS platform to simulate the mass movement process before and after treatment. This paper also provided the conditions and characteristic parameters of soil deposits (thickness flow height, speed velocity, and stresses) during the landslide mass movement process and mapped the 3D division of hazard zones before and after landslide treatment. Results indicated that the scope of hazard zones contracted after engineering treatment of the landslide. The extent of high-hazard zones was reduced by about 2/3 of the area before treatment, and characteristic parameters of the mass movement process after treatment decreased to 1/3 of those before treatment. Despite engineering treatment, the Tazhiping landslide still poses significant hazard to nearby settlements. Therefore, we propose that houses located in high-hazard zones be relocated or reinforced for protection.

Keywords: finite volume method; rheological model; motion feature parameters; hazard assessment

1. Introduction

The hazards of a landslide include scope of influence (i.e., source area, possible path area, and backward and lateral expansion area) and secondary disasters (i.e., reservoir surge, blast, and landslide-induced barrier lake). A typical landslide hazard assessment aims to propose a systematic hazard assessment method with regard to a given position or a potential landslide. Current research on typical landslide hazard assessment remains immature, and there are multiple methods for interpreting landslide hazards. To be specific, the scope of influence prediction of a landslide refers to deformation and instability characteristics such as sliding distance, movement speed, and bulking thickness range. The movement behavior of a landslide mass is related to its occurrence, sliding mechanisms, mass characteristics, sliding path, and many other factors. Current landslide movement prediction methods include empirical prediction and numerical simulation.

Empirical prediction method: The empirical prediction method involves

[a1]: Answer to the comment Q2: The title of this paper has been revised.

44 analyzing landslide flow through the collection of landslide parameters in the field. It
45 further consists of the geomorphologic method (Costa, 1984; Jackson et al., 1987;
46 Scott et al., 1993), the geometric change method (Zhang et al., 1994-1993; Finlay et
47 al., 1999; Michael-Leiba et al., 2003), and the volume change method (Fannin et al.,
48 2001). Empirical models are commonly simple and easy to apply, and the required
49 data are easy to obtain as well. **Numerical simulation method:** Numerical simulation
50 methods are further divided into the continuous deformation analysis method (Hung,
51 1995; Evans et al., 2009; Zhang, Y., 2013; Wang, L., et al., 2016), the discontinuous
52 deformation analysis method (Shi, G.H., 1988; Yin et al., 2002), and the simplified
53 analytical simulation method (Christen et al., 2010a; Sassa, 2010; Bartelt et al., 2012;
54 Du et al., 2015). The numerical simulation method expresses continuous physical
55 variables using the original spatial and temporal coordinates with geometric values of
56 discrete points. Numerical simulations follow certain rules to establish an algebraic
57 equation set in order to obtain approximate solutions for physical variables.

58 Empirical prediction models only provide a simple prediction of the sliding path.
59 Due to the differences in geological environments, empirical prediction models
60 commonly have low generality. The continuous deformation method has the
61 advantage of an extremely strong replication capability, but it is not recommended
62 when analyzing flow-type landslides ~~debris flows~~, lahars, or debris flows because of
63 complicated rheological behaviors (Iverson et al., 1997, 2001; Hung et al., 2001;
64 Glade 2005; Portilla et al., 2010; Chen et al., 2014). The fluid mechanics-based
65 discontinuous deformation method has several shortcomings such as, great
66 computational burden, difficult parameter selection, and difficult 3D implementation.
67 The simplified analytical simulation method fully takes into account the flow state
68 properties of landslides before introducing a rheological model and can easily realize
69 3D implementation on the GIS platform. On that account, this paper adopted the
70 continuous fluid mechanics-based finite volume method (simplified analytical
71 simulation method). We introduce a rheological model on the basis of using mass as
72 well as momentum and energy conservation to describe the movement of landslides.
73 We also employed GIS analysis to simulate the entire movement process of Taziping
74 landslide and map the 2D division of hazard zones.

75

76 2. Methods

77 2.1 Kinetic analysis method

78 Adopting the continuous fluid mechanics-based finite volume method, this paper
79 took into account erosion action on the lower surface of the sliding mass and the
80 change in frictional resistance within the landslide-debris flow in order to establish a
81 computational model. The basic idea is to divide the calculation area into a series of
82 non-repetitive control volumes, ensuring that there is a control volume around each
83 grid point. Each control volume is then integrated by the unresolved differential
84 equation in order to obtain a set of discrete equations. The unknown variable is the
85 numerical value of the dependent variable at each grid point. To solve the integral of a
86 control volume, we make a hypothesis about the change rule of values among grid

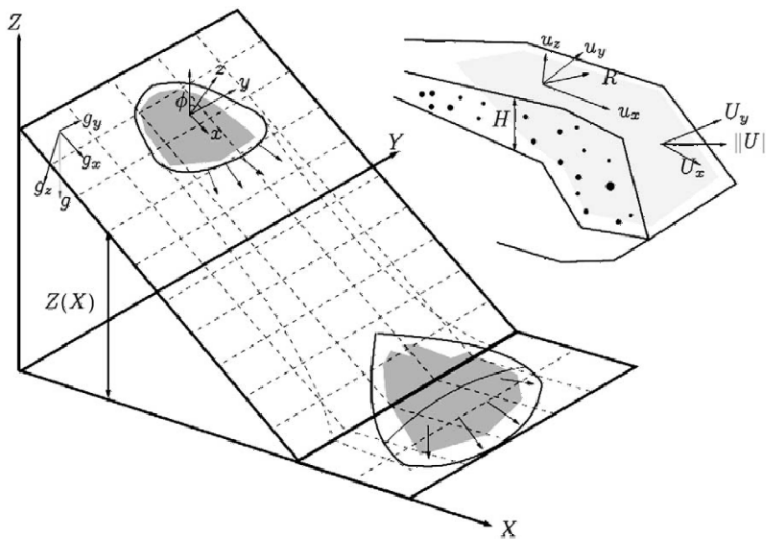
[a2]: Answer to the comment Q7: It has been revised. We have revised all references and quotations in the manuscript according to the NHESD journal style.

[a3]: Answer to the comment Q7: It has been revised.

[a4]: Answer to the comment Q7: It has been revised.

87 points, that is, about their piecewise distribution profile. The finite volume method
 88 can satisfactorily overcome the finite element method's weakness of slow calculation,
 89 and solve the problem of complex region processing. Thus, we adopted the finite
 90 volume method to establish the kinematic model for the landslide flow process.

91 The core of the finite volume method is domain discretization. The finite volume
 92 method uses discrete points as a substitute for continuous space. The physical
 93 meaning of the discrete equation is the conservation of the dependent variable in a
 94 finite control volume. Establishment of the conservation equation is based on the
 95 continuous movement model, that is, the continuity hypothesis about landslide
 96 substances. We divided the landslide mass into a series of units and made the
 97 hypothesis that each unit has consistent kinematic parameters (speed at a depth,
 98 density, etc.) and physical parameters (Fig.1). We also established an Eulerian
 99 coordinate system-based conservation equation with regard to each control volume.



100
 101 Fig.1 Schematic diagram of finite volume discretization (Christen et al., 2010a).

102 **2.2 Control equation**

103 The computational domain is defined as directions x and y , and the
 104 topographic elevation is given the coordinate $z(x, y)$. $H(x, y, t)$ is assumed as the
 105 change relationship of landslide thickness with time; $U_x(x, y, t)$ and $U_y(x, y, t)$
 106 respectively represent the mean movement speeds along directions x and y at
 107 moment t ; $n_x = U_x / \sqrt{U_x^2 + U_y^2}$ and $n_y = U_y / \sqrt{U_x^2 + U_y^2}$ represent the cosinoidal and
 108 sinusoidal flow vectors of the landslide on the plane $x-y$. The mean flow speed of

[a5]: Answer to the comment Q8: It has been revised (Christen et al., 2010a).

109 substances is defined as $U = \sqrt{U_x^2 + U_y^2}$.

110 Thus, the mass balance equation becomes:

$$111 \quad \partial_t H + \partial_x (HU_x) + \partial_y (HU_y) = \dot{Q} \quad (1)$$

112 wherein, $\dot{Q}(x, y, t)$ represents the change rate (entrainment rate) of landslide
113 volume with time.

114 Assuming that $l(x, y, t)$ represents the movement distance of the landslide with
115 time, we can obtain:

$$116 \quad \dot{Q} = \begin{cases} 0 & \text{if } h_i = 0 \\ \frac{\rho_i}{\rho_a} h_i \frac{U}{l} & \text{if } k_i l \geq h_i \\ \frac{\rho_i}{\rho_a} k_i U & \text{if } k_i l < h_i \end{cases} \quad (2)$$

117 wherein, h_i represents the thickness of the i th layer of the landslide in the
118 movement process; ρ_i represents the density of the i th layer of the landslide in the
119 movement process; ρ_a represents the density of the landslide; the dimensionless
120 parameter k_i represents the entrainment rate.

121 The momentum balance equation is:

$$122 \quad \partial_t (HU_x) + \partial_x (HU_x^2 + \frac{g_x k_{a/p} H^2}{2}) + \partial_y (HU_x U_y) = S_{gx} - S_f(R) [n_x] \quad (3)$$

$$123 \quad \partial_t (HU_y) + \partial_y (HU_y^2 + \frac{g_y k_{a/p} H^2}{2}) + \partial_x (HU_x U_y) = S_{gy} - S_f(R) [n_y] \quad (4)$$

124 wherein, $S_{gx} = g_x H$ and $S_{gy} = g_y H$ represent the dynamic components of the
125 acceleration of gravity in directions x and y ; $g = (g_x \ g_y \ g_z)$ represents the
126 vector of the acceleration of gravity; $k_{a/p}$ represents the pressure coefficient of soil;
127 ρ_a represents the density of the landslide; the dimensionless parameter k_i
128 represents the entrainment rate; $S_f(R)$ represents the frictional resistance.

129 The kinetic energy balance equation is:

$$130 \quad \partial_t (HR) + \partial_x (HRU_x) + \partial_y (HRU_y) = \dot{P} - \dot{D} \quad (5)$$

131 wherein, $R(x, y, t)$ represents the random mean kinetic energy of the landslide;
 132 $\dot{P}(x, y, t)$ and $\dot{D}(x, y, t)$ represent the random increased kinetic energy and decreased
 133 kinetic energy of the landslide.

134 **2.3 Constitutive relationship**

135 The improved Voellmy rheological model is applied in the computational
 136 simulation of the landslide. See the computational formula below:

$$137 \quad S_f = \frac{u_i}{\|U\|} (h\mu g_z + R_i U^2 + R_\zeta U^2) \quad (6)$$

$$138 \quad R_i = \mu h \frac{U^T K U}{U^2}, R_\zeta = \frac{g}{\zeta} \quad (7)$$

139 wherein, $u_i/\|U\|$ represents the unit vector in the movement direction of the
 140 landslide; μ represents the Coulomb friction coefficient, and is related to $R(x, y, t)$,
 141 the random mean kinetic energy of the landslide; R_i represents the gravity-related
 142 frictional force coefficient; K represents the substrate surface curvature; ζ
 143 represents the viscous friction coefficient of the ‘‘turbulent flow’’.

144 **2.4 HLLC-Heun numerical solution**

145 Synthesizing control equations (1), (3), (4) and (5), we can obtain the simplified
 146 form of the nonlinear hyperbola equation:

$$147 \quad \partial_t V + \nabla \cdot F(V) = G(V) \quad (8)$$

$$148 \quad V = \begin{pmatrix} H \\ HU_x \\ HU_y \\ HR \end{pmatrix} \quad G(V) = \begin{pmatrix} \dot{Q} \\ S_{gx} - S_{fx} \\ S_{gy} - S_{fy} \\ \dot{P} - \dot{D} \end{pmatrix}$$

$$149 \quad F(V) = \begin{pmatrix} HU_x & HU_y \\ HU_x^2 + g_z k_{ap} \frac{H^2}{2} & HU_x U_y \\ HU_x U_y & HU_y^2 + g_z k_{ap} \frac{H^2}{2} \\ HRU_x & HRU_y \end{pmatrix}$$

150 wherein, $V(x, y, t)$ represents a vector equation consisting of four unknown
 151 vector variables; $F(V)$ represents the flux function; $G(V)$ represents the source
 152 term. Based on the HLLC equation of the finite volume method and the quadrilateral
 153 grid, the node layout can adopt the grid center pattern, and the normal flux along one
 154 side of the control volume can be represented by the flux at the center of the side. The

155 finite volume discretization adopting the control volume as unit is depicted in Fig.1;
 156 the Gauss theorem can be followed for the integration of equation (8), wherein C_i
 157 represents the unit volume; after converting the volume integral flux function $F(V)$
 158 into the curved surface integral, we can obtain:

$$159 \quad \int_{C_i} \partial_i V dx + \iint_{\partial C_i} F(V) \cdot n_i d\sigma = \int_{C_i} G(V) dx \quad (9)$$

160 wherein, n_i represents the outward normal direction vertical to unit C_i at the
 161 boundary; through adopting the HLL format for the discretization of surface integral,
 162 the following simplified form can be obtained:

$$163 \quad V_i^{(*)} = V_i^{(n)} + \frac{\Delta t}{A_{C_i}} \Delta F_i^{(HLL)}(V^{(n)}) \quad (10)$$

$$164 \quad V_i^{(**)} = V_i^{(*)} + \frac{\Delta t}{A_{C_i}} \Delta F_i^{(HLL)}(V^{(*)}) \quad (11)$$

$$165 \quad V_i^{(n+1)} = \frac{1}{2} (V_i^{(n)} + V_i^{(**)}) \quad (12)$$

166 wherein, $V_i^{(n)}$ represents the mean value of unit variables at moment $t^{(n)}$; $V^{(n)}$
 167 represents the mean value of the entire grid at moment $t^{(n)}$; $\Delta t := t^{(n-1)} - t^{(n)}$ represents
 168 the calculated time step; A_{C_i} represents the area of unit C_i ; $\Delta F_i^{(HLL)}$ represents the
 169 approximate value of the curved surface integral, as shown below:

$$170 \quad \Delta F_i^{(HLL)}(V^{(n)}) := - \sum_{j=1}^4 F_{ij}^{(HLL)}(V^{(n)}) n_{ij} \Delta X \quad (13)$$

171 wherein, n_{ij} represents the outward normal direction of the i th unit at
 172 boundary j ; the flux calculation term $F_{ij}^{(HLL)}(V^{(n)})$ represents the approximate
 173 solution mode of the Riemann problem of the i th unit at boundary j ; see the
 174 computational formula below:

$$175 \quad F_{ij}^{(HLL)}(V^{(n)}) = \begin{cases} F(V_L^{(n)}) & 0 \leq S_L \\ \frac{S_R F(V_L^{(n)}) - S_L F(V_R^{(n)}) + S_R S_L F(V_R^{(n)} - V_L^{(n)})}{S_R - S_L} & S_L \leq 0 \leq S_R \\ F(V_R^{(n)}) & S_R \leq 0 \end{cases} \quad (14)$$

176 wherein, $V_L^{(n)}$ and $V_R^{(n)}$ respectively represent the approximate values of $V^{(n)}$

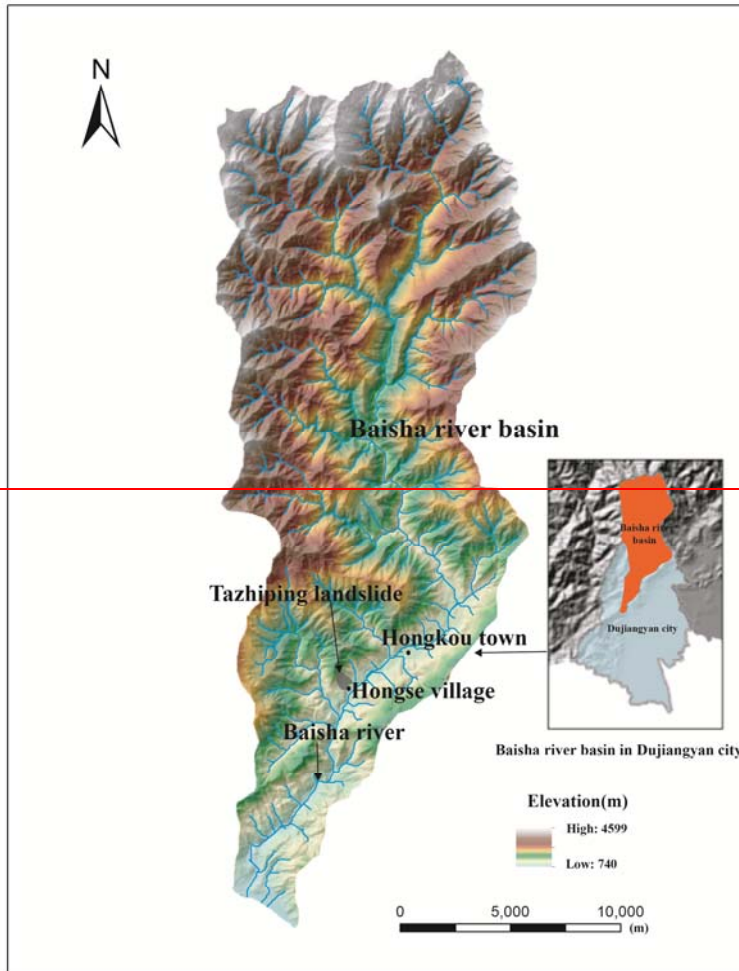
177 on both sides of boundary j of the i th unit; S_L and S_R respectively represent the
178 wave speeds on the left and right sides. Refer to the computational method described
179 by Toro (1992). In addition, the gradient magnitude in the original second-order
180 difference equation can be limited through multiplication with the flux limiter, and the
181 second-order format of the TVD property can be constructed to avoid the occurrence
182 of numerical oscillation. Refer to the specific method described by LeVeque (2002).

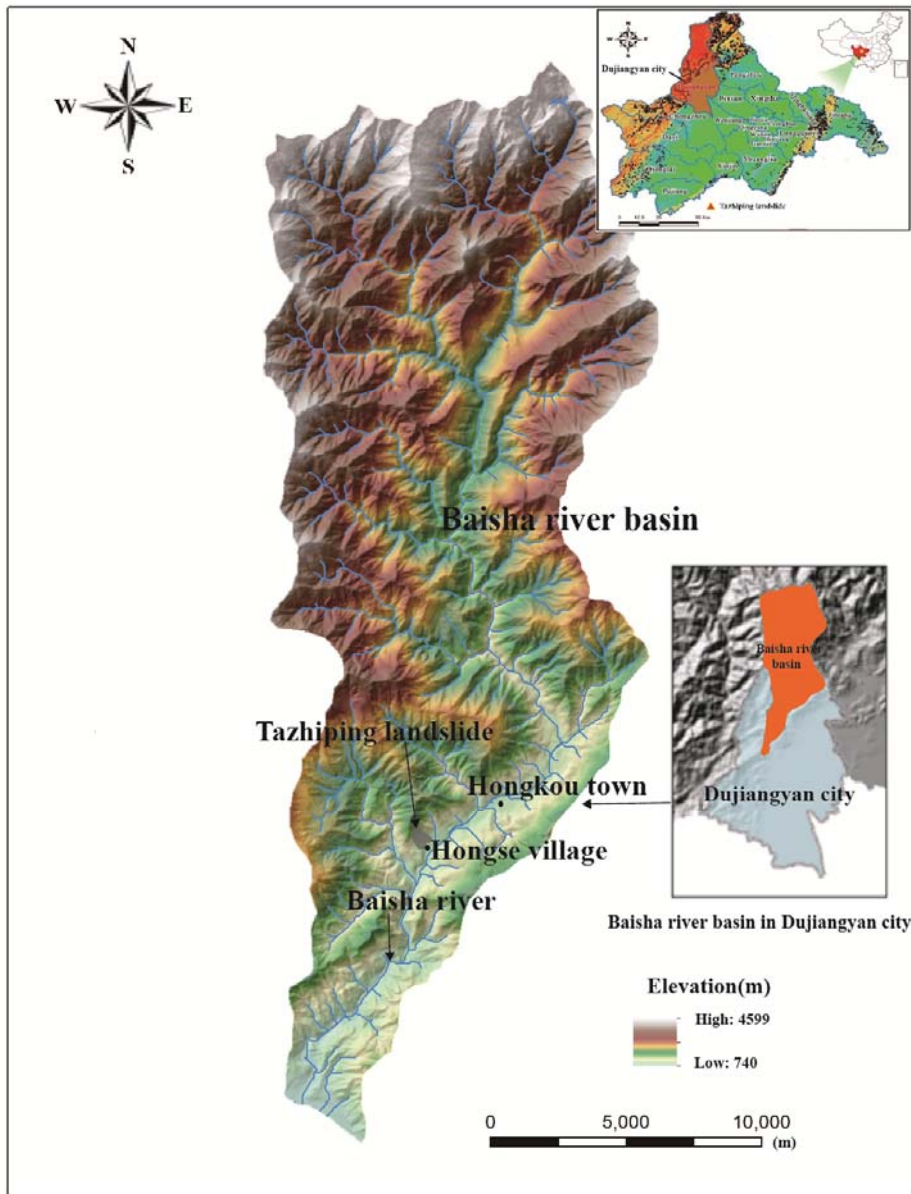
183 In this paper ~~a numerical solver used~~ within RAMMS is used, which was
184 specifically designed to provide landslide (avalanche) engineers with a tool that can
185 ~~be applied to~~ analyze problems ~~that with~~ two-dimensional depth-averaged mass and
186 momentum equations on three-dimensional terrain using both first and second-order
187 finite volume methods (Christen et al., 2010b).

188 3. Study area and data

189 3.1 Taziping landslide

190 The Taziping landslide is located ~~in the~~ southeast of the Hongse Village,
191 Hongkou Town, Dujiangyan City of Sichuan Province. The site is located at
192 (E103°37'46", N31°6'29"), 68 km ~~away from west~~ Chengdu City ~~to the east~~ and 20
193 km ~~away~~ from the Dujiangyan Urban District (Fig. 2). Its geomorphic unit is a
194 middle-mountain tectonic erosional area, ~~falling within the slope geomorphology~~ on
195 the north bank of the Baisha River Valley. ~~As an colluvial layer landslide triggered by~~
196 ~~the Wenchuan Earthquake,~~ The Taziping Landslide is a large-scale colluvial layer
197 landslide triggered by the Wenchuan Earthquake, ~~landslide as shown in~~ (Fig. 3). It has
198 a gradient of 25°-40° with an average gradient ~~of about~~ 32°. The landslide has an
199 apparent round-backed armchair contour, ~~and has formed with~~ a steep rear edge,
200 which has a gradient of 35°-50° and an elevation of about 1,370 m. The front edge is
201 located on the south side of the mountain road, and has an elevation of about 1,007 m.
202 The landslide has an elevation difference of about 363 m, and ~~the a~~ main sliding
203 direction of 124°NE. The landslide mass ~~is informs~~ an irregular semi-elliptical shape,
204 and has a length of about 530 m, an average width of 145 m and ~~an landslide~~ area of
205 approximately 7.68×10^4 m². The landslide mass is composed of gravelly soil ~~in~~
206 ~~lithology~~, and is covered on ~~the surface~~ by silty clay mingled with gravels. In terms of
207 spatial distribution, ~~it the landslide~~ is thick in the middle and thin on the lateral edges,
208 ~~and~~ has a thickness of 20-25 m and a volume of approximately 1.16×10^6 m³. During
209 the earthquake, the landslide mass slid to cover the northern mountain slope ~~mass~~ of
210 the Hongse Village Miaoba settlement. The landslide has an apparent front edge
211 boundary, and there is also a swelling deformation (Fig. 4).



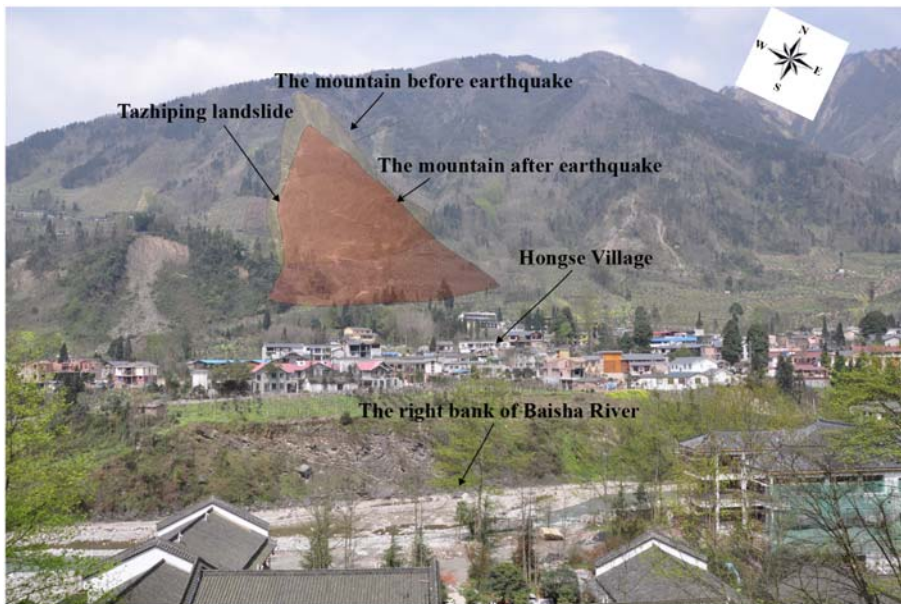


213

214

215

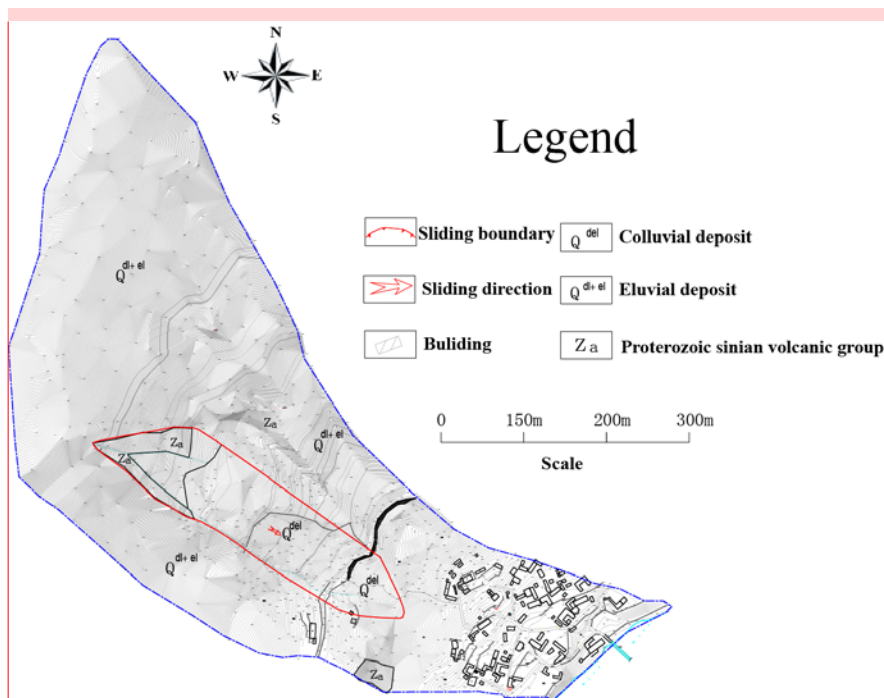
Fig.2 Location of Tazhiping landslide, Baisha river basin, Dujiangyan city (the landslide was triggered by Wenchuan Ms 8.0 earthquake on May 12, 2008)



216

217

Fig.3 Taziping Landslide



218

219

220

221

222

Fig.4 Plane sketch of the Tazhiping landslide

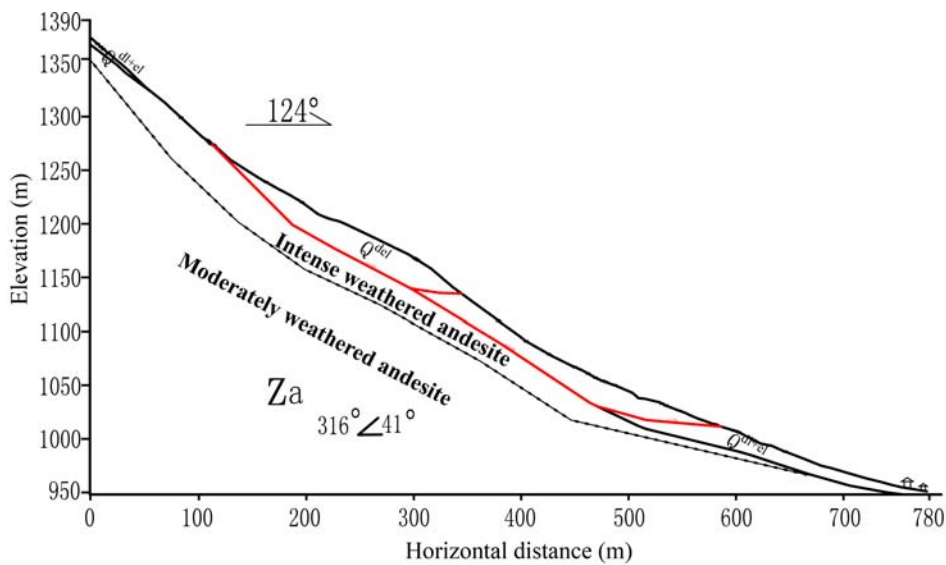
After the Wenchuan Earthquake, the massive colluvial deposits covers covered on the mountain slope, and the landslide mass is dominated by the colluvium. The colluvium is mainly distributed on the top surface of the landslide mass in the

[a6]: Answer to the comment Q4: We have reconstructed and added Figure4.

223 ~~thickness of 0.5-5.0 m thick at the top of the slide,~~ and is ~~mainly constituted~~
 224 ~~by composed of~~ rubbles and gravels. The mass consists of a small amount of fine
 225 gravel, ~~substances which are is composed of~~ gray or grayish-green, ~~and dominated by~~
 226 andesite ~~in composition, generally~~ with a ~~block size~~ ~~clast~~ of 20-150 cm. Field surveys
 227 indicates that the rubbles in the surface layer ~~have has~~ a maximum diameter
 228 exceeding 2 m, and that fine gravel ~~substances are filled among rubbles in a loose~~
 229 ~~structure is loosely intercalated with the rubble. Within the thickness of 5-10 m, the~~
 230 ~~landslide mass is constituted of a~~ small amount of yellowish-brown and gray-brown
 231 silty clay ~~mingled mixed~~ with 5-40% of non-uniformly distributed ~~broken~~ rubble
 232 ~~composed the first 5-10 m of the slide.s Within the thickness of~~ From 10-25 m ~~deep,~~
 233 there is a wide distribution of gravelly soil. The soil is grayish-green or variegated in
 234 color, is slightly compact and non-uniform, and has a ~~broken stone~~ ~~rock fragment~~
 235 content of about 50%. The parent rock of the ~~broken stone~~ ~~rock fragments~~ is andesite,
 236 filled with silty clay or silt (Fig.4 5). Table 1 shows the parameters of the surface
 237 gravelly soil of the landslide mass based on the field sampling.

238 Tab.1 Parameters of ~~the~~ surface soil of Taziping Landslide

Internal friction angle (°)		Cohesion (kPa)	Relative compactness	Natural void ratio	Dry density (kN·m ⁻³)	Specific gravity (g·cm ⁻³)
Peak	Residual					
27.5	23	20.5	53%	0.789	15.357	2.492



239 slide surface Q^{del} colluvial deposit Q^{dl^rel} eluvial deposit Z_a proterozoic sinian volcanic group

240 Fig.4-5 Geological profile of the Taziping Landslide

241 The landslide is an unconsolidated mass containing relatively large amounts of
 242 crushed stones and silty clay (Fig.5 6). Its loose structure and strong permeability
 243 facilitate infiltration of surface water. The Wenchuan earthquake aggravated the

244 deformation of the landslide making deposits more unconsolidated, further reducing
245 the stability of the landslide mass. During persistent rainfall, surface water infiltrates
246 the landslide slope resulting in increased water pressure within the landslide mass and
247 reduced shear strength on the sliding surface. Thus, rainfall constitutes the primary
248 inducing factor of the upper Taziping landslide. After infiltrating the loose layer, water
249 saturates the slope increasing the dead weight of the sliding mass and reducing the
250 shear strength of soil in the sliding zone. Infiltration into the landslide mass also
251 increases the infiltration pressure of perched water, drives deformation, and poses a
252 great threat to villages located at the front of the landslide. Slide-resistant piles and
253 backfill were placed at the toe of the slope in order to reduce the hazards of future
254 slides. The slide-resistant piles have enhanced the overall stability of the slope,
255 however, under heavy rainfall the upper unconsolidated landslide deposits may cut
256 out from the top of the slide-resistant piles.



257 (a) Material on the landslide surface (b) Material in the shear zone

258 Fig.5-6 Photographs showing Colluvial-colluvial deposits covers on the mountain
259 slope

260
261 Therefore we simulate possible movement states of the Taziping landslide before
262 and after treatment with slide-resistant piles, comparatively analyzed the kinetic
263 parameters in the movement process, and mapped the 3D division of hazard zones.

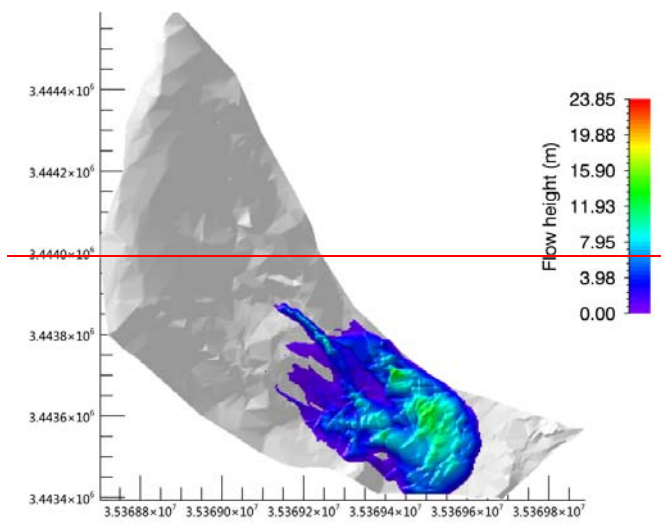
264 3.2 Hazard prediction before treatment

265 It was assumed that the landslide was damaged before engineering treatment.
266 According to field investigation, the sliding mass had an estimated starting volume of
267 about $600,000\text{m}^3$ and a mean thickness of 8m. Based on the survey report and field
268 investigation (Hydrologic Engineering and Geological Survey Institute of Hebei
269 Province, 2010), we adopted the survey parameters of Tab.2 for the simulated
270 calculation. These parameters were obtained from laboratory or small-scale
271 experiments and back-analyses of relatively well-documented landslide cases. The
272 unit weigh $\gamma = 20.8\text{kN} \cdot \text{m}^{-3}$ is from small-scale conventional
273 triaxial test experiments in laboratory. In addition, we selected the coulomb friction
274 coefficient $\mu = 0.45$ and viscous friction coefficient $\zeta = 500\text{m} \cdot \text{s}^{-2}$ in accordance
275

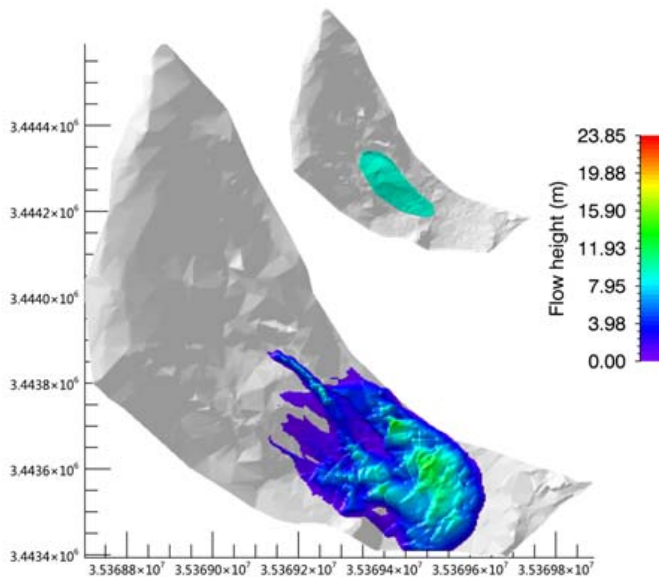
276 with back-analyses of well-documented landslide cases (Cepeda et al., 2010; Du et al.,
 277 2015). The erosional entrainment rate selected was the minimum value $k_i = 0.0001$
 278 in the RAMMS program.

279 Tab.2 Model calculation parameters

Unit weight $\gamma(kN \cdot m^{-3})$	Coulomb friction coefficient μ	Viscous friction coefficient $\zeta(m \cdot s^{-2})$	Erosional entrainment rate k_i
20.8	0.45	500	0.0001



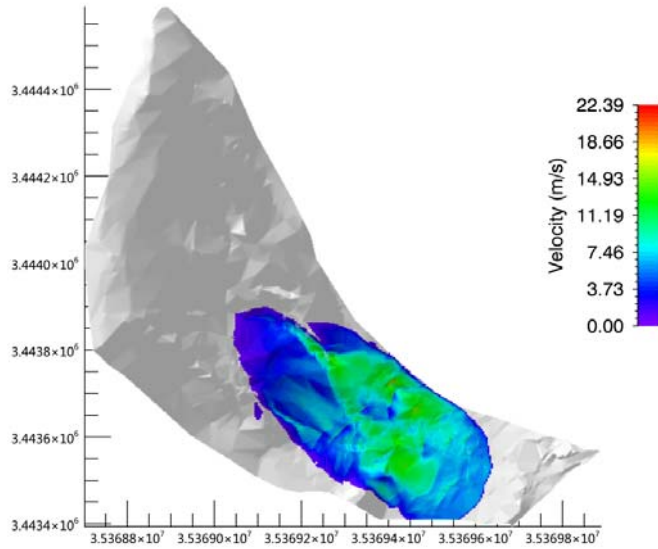
280



281

282

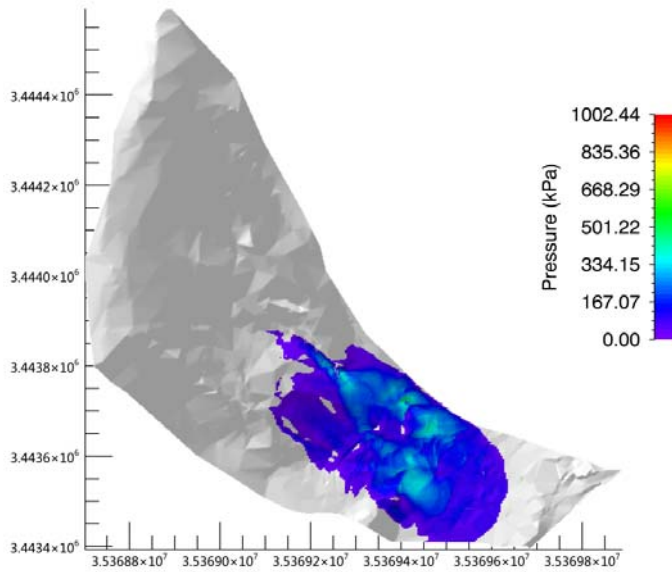
(a) ~~Thickness~~ Flow height



283

284

(b) ~~Speed~~ Velocity



285

286

(c) Pressure

287 Fig.67 Movement characteristic parameters of the Taziping landslide (before
288 treatment)

289 See the kinematic characteristic parameters of the landslide deposits in Fig.6 7.
290 The colored bar shows the maximum values of the kinematic process for a given
291 step. As shown by the calculation results, ⊕ deposits accumulated during the

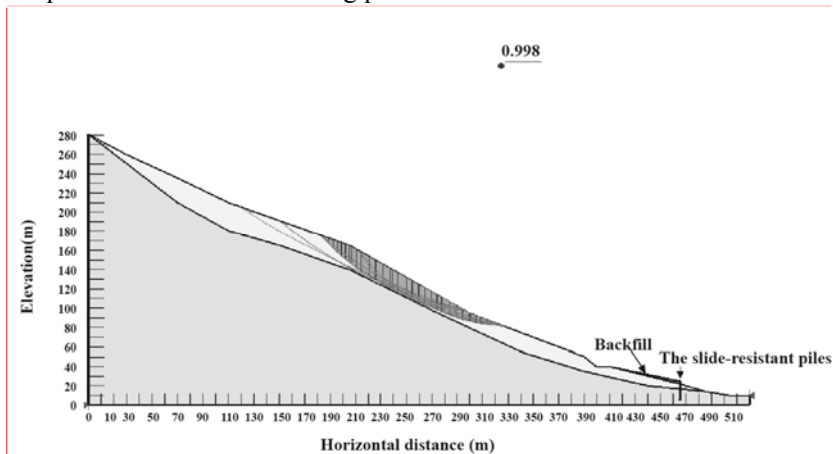
[a7]: Answer to the comment Q9:
Figure.7 is shown that the last moment of the flow. Different moment have different deposit flow height, velocity and pressure. However, the coloredbar shows the maximum values of moving process or an instantaneous for a given time step. It has been revised.

292 landslide movement process had a maximum **thickness flow height** of 23.85m, located
 293 around the surface gully of the middle and upper slope. **The middle and lower section**
 294 **of the landslide deposits** had a **thickness flow height** of about 5-10m; ② the middle
 295 and lower movement **speed velocity** of the landslide ranged from 3m/s and 7m/s; ③
 296 the landslide had a mean pressure of about 500kPa, and the pressure of the middle and
 297 lower deposits was about 200kPa. Thus, three-story and lower houses within the
 298 deposition range might be buried, and it was further suggested that the design strength
 299 of the gable walls of houses on the middle and upper parts of the deposit be increased
 300 above 300kPa.

301

302 3.3 Hazard prediction after treatment

303 After fully accounting for the slide-resistant piles and mounds, we introduced the
 304 Morgenstern-Price method (Morgenstern et al., 1965) to calculate the stability
 305 coefficient of Taziping landslide after treatment. **The method was determined with an**
 306 **iterative approach by changing the position of the sliding surface until failure of the**
 307 **dumpsite (Fig.8).** The physico-mechanical parameters under a saturated state
 308 (Hydrologic Engineering and Geological Survey Institute of Hebei Province, 2010)
 309 were adopted to search for the sliding plane of the landslide.



310

311 **Fig.8 Search for the sliding plane of the Taziping landslide (after treatment)**

312 **Based on numerical analysis, the Taziping landslide stability coefficient is 0.998.**
 313 Under rainfall conditions, the middle area of the Taziping landslide was unstable.
 314 Loose deposits in the middle part of the landslide might convert into a high-water
 315 landslide substances and cut out from the top of the slide-resistant piles. In the
 316 damaged area, the slope had a rear edge wall elevation of about 1,170m. Its front edge
 317 was located on the south side of the mountain road, with an elevation of **about 1,070m**
 318 **1,070-1,072m** and a length of **about 180m** ~~180m~~ **182m**. Thus, the scale of the
 319 rainfall-damaged is estimated to be about 250,000m³, with a mean thickness of about
 320 6m. The parameters in Tab.2 were again adopted for the simulated calculation.

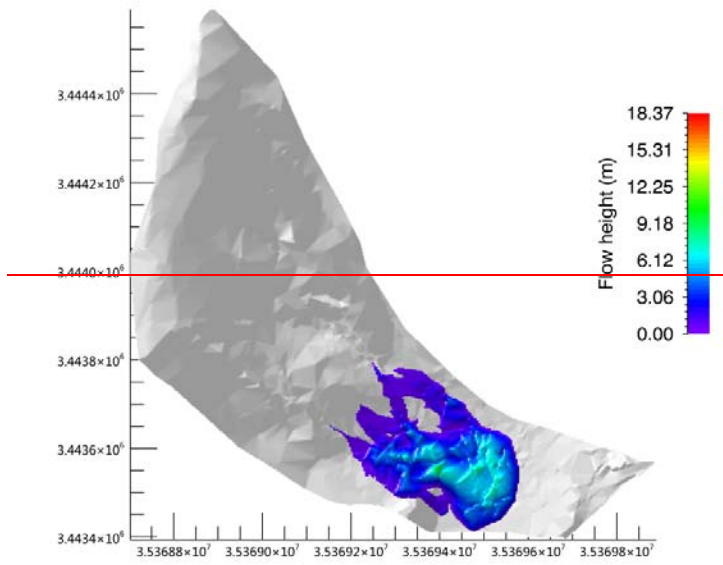
[a8]: Answer to the comment Q10:
 This sentences has been reformulated, because of wrong word order.

[a9]: Answer to the comment Q5 and Q11: Before engineering treatment, Figure.4 and Figure.5 have showed that the sliding mass had an estimated starting volume of about 600,000m³ and a mean thickness of 8m. After fully accounting for the slide-resistant piles and mounds, we introduced the Morgenstern-Price method to calculate the stability coefficient of Taziping landslide after treatment. The method was determined with an iterative approaching by changing the position of the sliding surface until failure of the dumpsite (Figure.8)

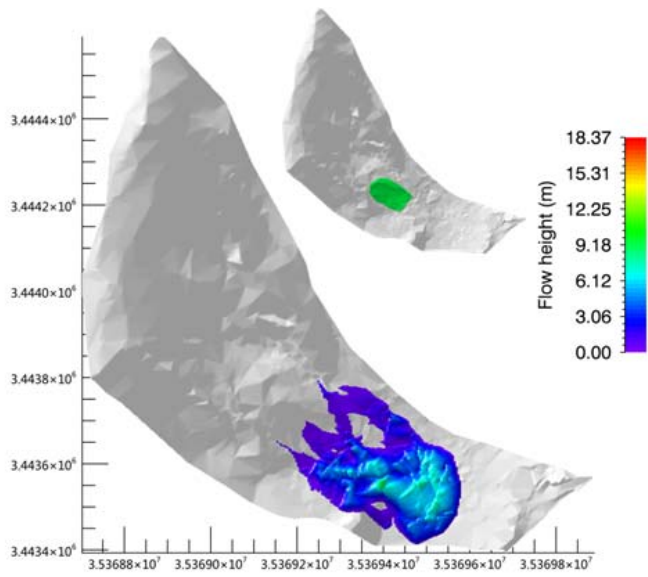
[a10]: Answer to the comment Q5:
 We have reconstructed and added Figure8.

[a11]: Answer to the comment Q5:
 The result of numerical analysis.

321

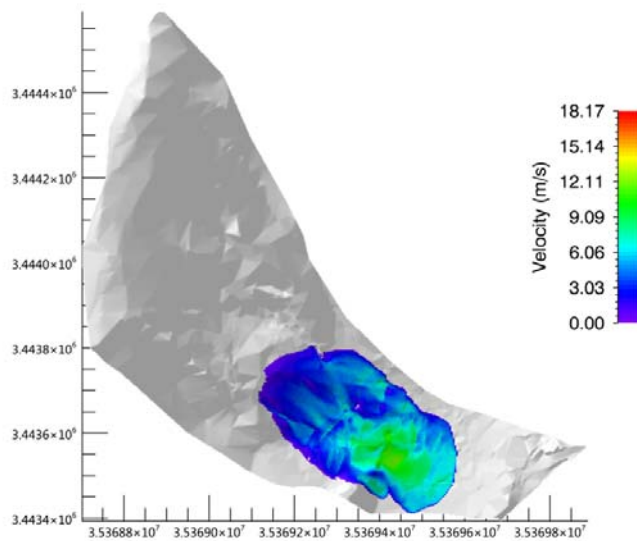


322

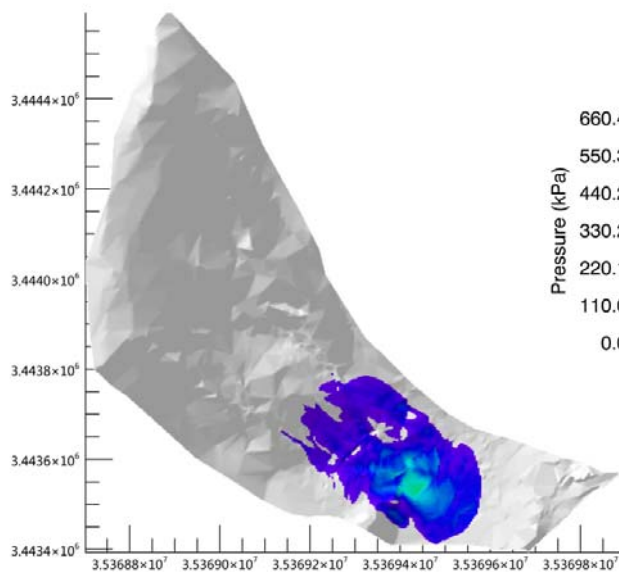


323

(a) ~~Thickness~~ Flow height



(b) Speed Velocity



(c) Pressure

324
325

326
327

Fig.7 9 Movement characteristic parameters of the Taziping landslide (after treatment)

Provided in Fig.4 9 are the kinematic characteristics of the landslide deposit. The coloredbar shows the maximum values of moving process or an instantaneous for a given time step. ① Deposits accumulated during the landslide movement process had a maximum thickness flow height of 18.37m, located around the surface gully of the middle and upper slope. The middle and lower portions of the landslide deposits had a thickness flow height of approximately 3-5m. ② The middle and lower movement

328
329
330
331
332
333
334

[a12]: Answer to the comment Q12: It has been revised.

[a13]: Answer to the comment Q9: Figure.9 is shown that the last moment of the flow. Different moment have different deposit flow height, velocity and pressure. However, the coloredbar shows the maximum values of moving process or an instantaneous for a given time step. It has been revised.

[a14]: Answer to the comment Q10: This sentences has been reformulated, because of wrong word order.

335 ~~speed~~ velocity of the landslide deposits ranged between 3m/s and 5m/s. ③-The
 336 landslide had a mean pressure of about 330kPa, and the pressure of the middle and
 337 lower deposits was about 100kPa. Thus, it could be held that two-story and lower
 338 houses within the deposition range might be buried. It ~~was-is~~ further suggested that
 339 the design strength of the gable walls of houses on the middle and upper parts of the
 340 deposits be increased above 150kPa.

341 After treatment, the accumulation ~~thickness~~ flow height and pressure of the
 342 deposits were reduced by about 1/2, and the kinematic speed was reduced by about
 343 1/3. However, the Miaoba residential area of Red Village was still partially at hazard.
 344

345 4 Results

346 Landslides reflect landscape instability that evolves over meteorological and
 347 geological timescales, and they also pose threats to people, property, and the
 348 environment. The severity of these threats depends largely on landslide speed and
 349 travel distance. There may be examples where entire houses on a landslide mass are
 350 moved but not destroyed because of stable base plates. In any case, velocity plays a
 351 more important role regarding kinetic energy acting on an obstacle. However, the
 352 Miaoba residential area of Red Village is located at the frontal part of Tazhiping
 353 landslide. During landslide movement, the spatial scale indexes of a landslide mass
 354 include area, volume, and thickness. The maximum thickness of the landslide is one
 355 of the direct factors influencing the building's deformation failure status. A large
 356 landslide displacement may lead to burial, collapse, or deformation failure of the
 357 building, and thus influence its safety and stability. Thus, landslide thickness
 358 constitutes an important index for assessing the hazards of a landslide disaster, and for
 359 influencing the consequences faced by disaster-affected bodies (Fell et al., 2008;
 360 DZ/T, 0286-2015). Provided in Tab.3 is a landslide thickness-based division of the
 361 predicted hazard zones of Taziping landslide, in which the thickness of the landslide
 362 mass correlates with the ability of a building to withstand a landslide disaster (Hung
 363 et al., 1984; Petrazzuoli et al., 2004; Glade 2006; GB, 50010-2010; Hu et al., 2012;
 364 Zeng et al., 2015). After treatment with slide-resistant piles, the hazard of a future
 365 slide was reduced by about 1/3 overall and by 2/3 in high-hazard zones.

366 **Tab.3 Division table of the predicted hazards of Taziping landslide (unit: m²)**

Hazard zone level	Assessment index	Building damage probability	Area before treatment	Area after treatment	Increased/decreased area	Building damage characteristics
Low-hazard zone (I)	$h \leq 0.5m$	20%	44 , 600	38 , 748	-5,852	One-story houses may be damaged; houses on the

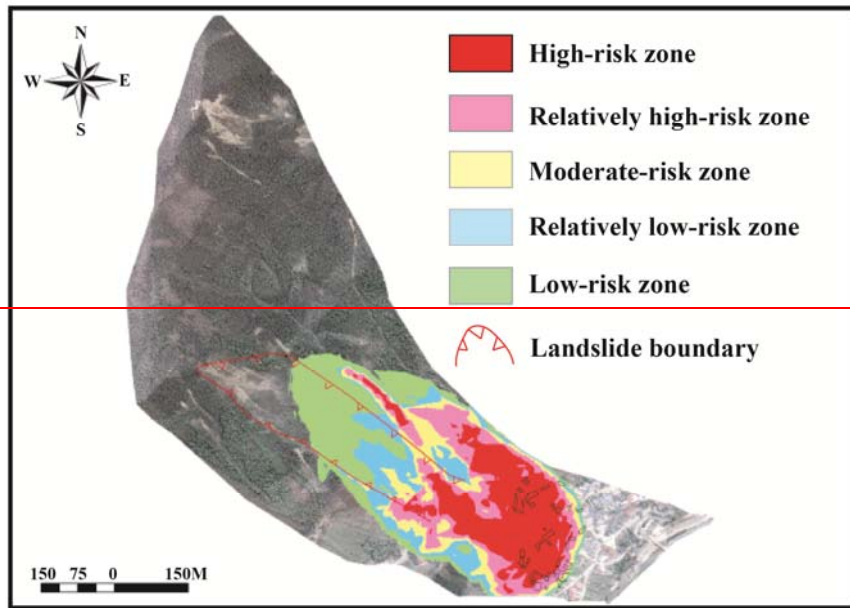
[a15]: Answer to the comment Q6: We have cited standard code and literature.

[a16]: Answer to the comment Q13:By the thickness of the landslide mass to evaluate the ability of a building to withstand a landslide disaster. We have cited relevant literatures.

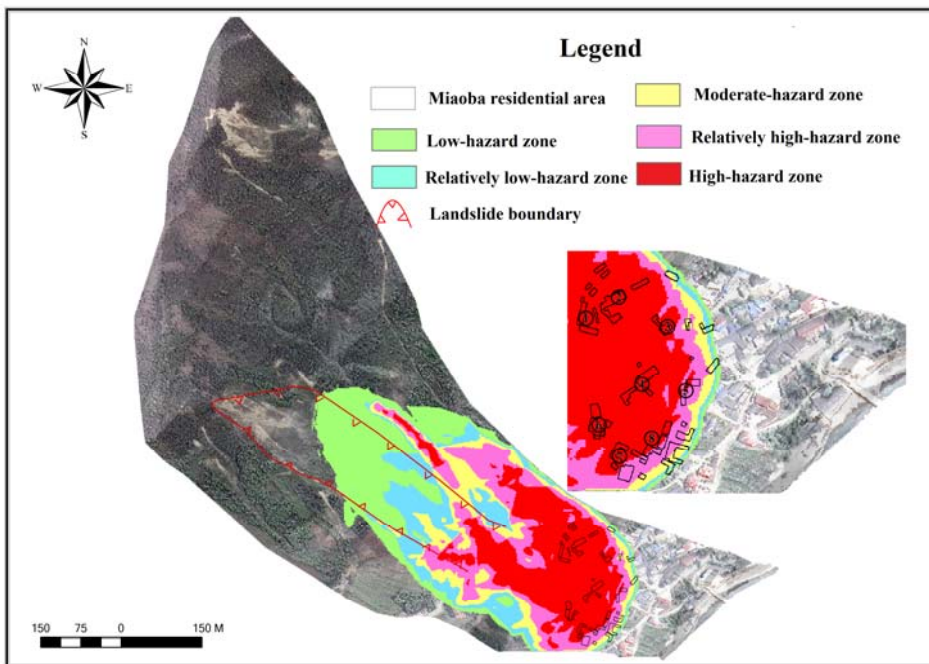
						landslide mass are partially damaged.
						One-story houses have a very high probability of being
Relatively low-hazard zone (II)	$0.5 \text{ m} < h \leq 1 \text{ m}$	50~20%	24 , 900	26 , 400	+1,500	washed away damaged; one-story houses on the landslide mass are completely damaged.
Moderate-hazard zone (III)	$1 \text{ m} < h \leq 3 \text{ m}$	80~50%	21 , 980	15 , 856	-6,124	One-story to three-story houses have a very high probability of being washed away damaged; houses less than three stories on the landslide mass are completely damaged.
Relatively high-hazard zone (IV)	$3 \text{ m} < h \leq 5 \text{ m}$	100~80%	30 , 820	19 , 636	-11,184	One-story houses may be buried, and two-story to six-story houses have a very high probability of being washed away

						damaged; houses on the landslide mass are completely damaged. Two-story and lower houses may be buried, and three-story and higher houses have a very high probability of being washed away damaged; houses on the landslide mass are completely damaged.
High-hazard zone (V)	$h \geq 5m$	100%	47 , 240	13 , 052	-34,188	
Total area:	—	—	169 , 540	113 , 700	-54,340	—

367 Given in Fig. 8 10 are the 3D divisions of hazard zones of the Taziping landslide
368 before and after engineering treatment. The scope-size of the hazard zones changed
369 before and after engineering treatment, particularly in the high-hazard zones. Before
370 treatment with slide-resistant piles, the landslide posed a great hazard to eight houses
371 on the left side of the upper Miaoba residential area, with a high-hazard zone
372 associated with landslide mass height over 5m and a red zone. After treatment, the
373 number of effected houses was reduced to four. We defined outside the colored area as
374 no-hazard.



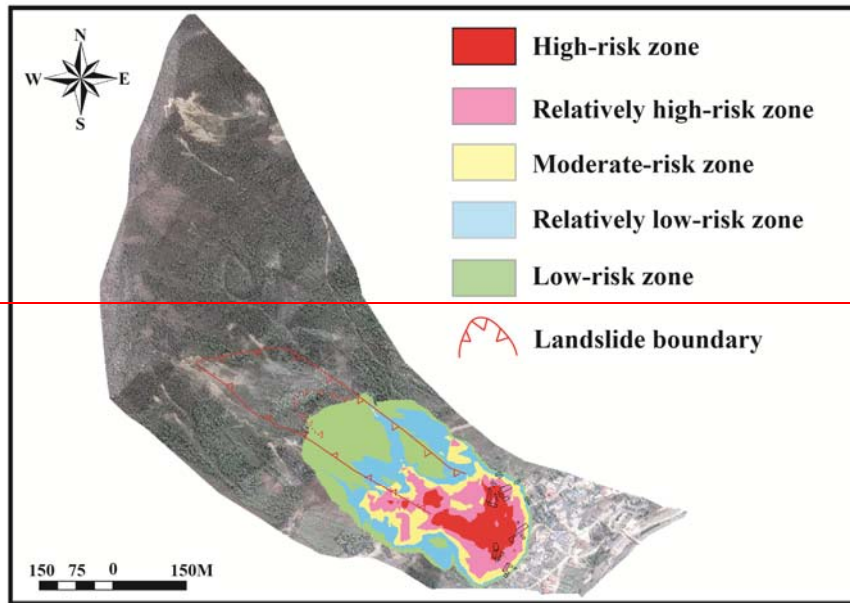
375



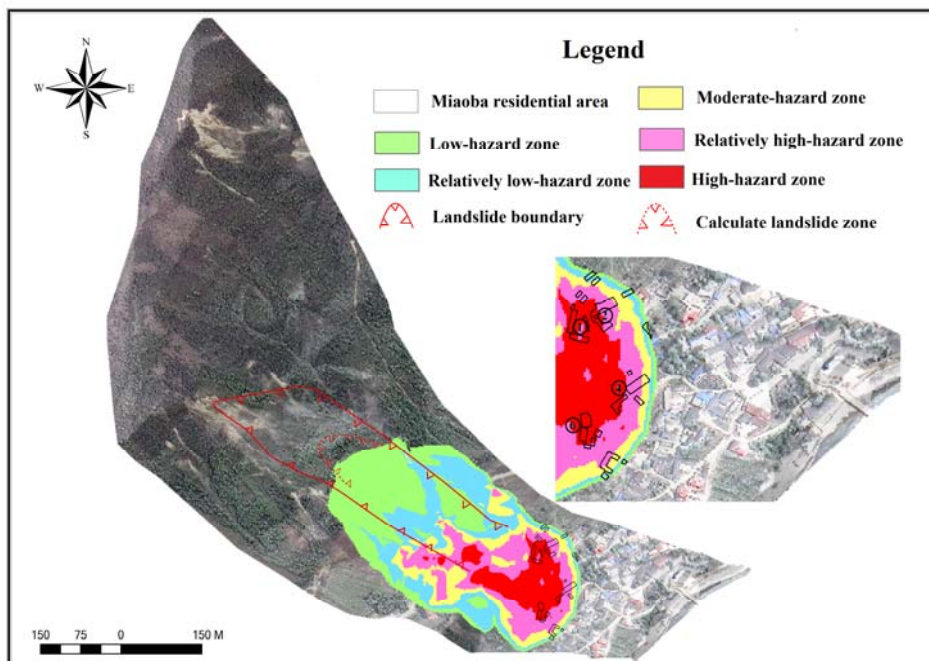
376

377

(a) Before treatment



378



379

(eb) After treatment

380

Fig.810 3D division comparison of the hazards of the Taziping landslide

381

382

5 Conclusions and Discussion

383

The hazard assessment of landslides using numerical models is becoming more and more popular as new models are developed and become available for both

384

385

386 scientific research and practical applications. There is some confusion about the mass
387 movement process that is discussed by the rheological model presented in this
388 contribution.

389 Landslides move downslope in many different ways (Varnes, 1978). In addition,
390 landslides can evolve into rapidly travelling flows, which exhibit characteristics of
391 debris flows on unchannelized or only weakly channelized hillslopes. The
392 geomorphic heterogeneity of rapid shallow landslides, such as hillslope debris flows,
393 is larger than observed in channelized debris flows; however many of these flows can
394 be successfully modelled using the Voellmy-fluid friction (Christen et al., 2012).
395 Results presented in this paper support the conclusion that Voellmy-fluid rheological
396 model can be used to simulate flow-type landslides.

397 The selection of model parameters remains one of the fundamental challenges
398 for numerical calculations of natural hazards. At present, there are numerous
399 empirical parameters obtained from 30-years of monitoring data. Such as in RAMMS,
400 we can automatically generate the friction coefficient of an avalanche for our
401 calculation domain based on topographic data analysis, forest information and global
402 parameters (WSL, 2013). The friction parameters for debris flows can found in some
403 literature (Fannin et al., 2001; Iovine et al., 2003; Hürlimann et al., 2008; Scheidl et
404 al., 2010; Huang et al., 2015). However, there is little research regarding friction
405 parameters of flow-type landslide. Therefore, we tested different coulomb friction
406 coefficient μ values ranging between $0.1 \leq \mu \leq 0.6$ and viscous friction coefficient ζ

407 values ranging between $100 \leq \mu \leq 1000 m \cdot s^{-2}$. Finally, we selected the coulomb

408 friction coefficient $\mu = 0.45$ and viscous friction coefficient $\zeta = 500 m \cdot s^{-2}$ in
409 accordance with back-analyses of well-documented landslides (Cepeda et al., 2010;
410 Du et al., 2015). Simulation results are consistent with field observations of
411 topography and sliding path.

412 Based on the finite volume method and program RAMMS, the simulation results
413 of Taziping landslide were consistent with the sliding path predicted by the field
414 investigation. This correlation indicates that numerical simulation is an effective
415 method for studying the movement processes of flow-type landslides—debris flows.
416 The accumulation thickness flow height and pressure of landslide deposits were
417 reduced by about 1/2, and the kinematic speed was reduced by about 1/3 after
418 treatment. However, the Miaoba residential area of Red Village is still partially at
419 hazard. Considering that two-story and lower houses within the deposition range
420 might be buried, it was further suggested that the design strength of the gable walls of
421 houses on the middle and upper parts of the deposit be increased above 150kPa.

422 By utilizing a GIS platform in combination with landslide hazard assessment
423 indexes, we mapped the 3D division of the Taziping landslide hazard zones before
424 and after engineering treatment. The results indicated that overall hazard zones
425 contracted after engineering treatment and, the area of high-hazard zones was reduced
426 by about 2/3. After engineering treatment, the number of at hazard houses on the left

[a17]: Answer to the comment Q3 :
This paper adopted the RAMMS to simulate the mass movement process. In RAMMS, we can automatically generate the friction coefficient for our calculation domain based on topographic data analysis, forest information and global parameters and so on. Therefore, we can use a changed frictional resistance. This problem has considered in the discussion section.

427 side of the upper Miaoba residential area, was reduced from eight to four. It was thus
428 clear that some zones are still at high hazard despite engineering treatment. Therefore,
429 it was proposed that houses located in high-hazard zones be relocated or reinforced
430 for protection.

431

432

433

434 **Acknowledgments**

435 The authors sincerely acknowledge the CAS Pioneer Hundred 432 Talents
436 Program for the completion of this research. This work was supported by National
437 Natural Science Foundation of China (Grant No. 41301009 41301592) and the
438 Hundred Young Talents Program of IMHE (SDSQB-2016-01), the International
439 Cooperation Program of the Ministry of Science and Technology of China (Grant
440 No.2013DFA21720). The authors express their deepest gratitude to those aids and
441 assistances. **The authors also extend their gratitude to editor and two anonymous**
442 **reviewers for their helpful suggestions and insightful comments, which have**
443 **contributed greatly in improving the quality of the manuscript.**

444

445

446 **Reference**

- 447 Bartelt, P., Bühler, Y., Buser, O., Christen, M., and Meier, L.: Modeling massdependent flow
448 regime transitions to predict the stopping and depositional behavior of snow avalanches, *J.*
449 *Geophys. Res.*, 117, F01015, doi:10.1029/2010JF001957, 2012 .
- 450 Costa, J.E.: Physical geomorphology of debris flows. *Developments and Applications of*
451 *Geomorphology*, Springer Press., 268-317, 1984.
- 452 Christen, M., Kowalski, J., and Bartelt, P.: RAMMS: Numerical simulation of dense snow
453 avalanches in three-dimensional terrain, *Cold Regions Science and Technology.*, 63, 1–14,
454 2010.
- 455 Christen, M., Bartelt, P., and Kowalski, J.: Back calculation of the In den Arelen avalanche with
456 RAMMS: interpretation of model results, *Annals of Glaciology.*, 51, 161–168, 2010.
- 457 Christen, M., Bühler, Y., Bartelt, P., Leine, R., Glover, J., Schweizer, A., Graf, C., McArdeall, B.,
458 Gerber, W., Deubelbeiss, Y., Feistl, T., and Volkwein, A.: Integral hazard management using a
459 unified software environment: numerical simulation tool “RAMMS” for gravitational natural
460 hazards, In: Koboltschnig, G., Hübl, J., Braun, J. (eds.) *Proceedings of 12th Congress*
461 *INTERPRAE.*, 1, 77–86, 2012.
- 462 Chen, J.C., and Chuang, M.R.: Discharge of landslide-induced debris flows: case studies of
463 Typhoon Morakot in southern Taiwan, *Nat. Hazards Earth Syst. Sci.*, 14, 1719-1730, 2014.
- 464 Cepeda, J., Chávez, J.A., and Martínez, C.C.: Procedure for the selection of runoff model
465 parameters from landslide back-analyses: application to the Metropolitan Area of San
466 Salvador, El Salvador, *Landslides.*, 7, 105–116, 2010.
- 467 Du, J., Yin, K.L., and Wang, J.J.: Simulation of three-dimensional movement of landslide-debris
468 flow based on finite volume method, *Chinese Journal of Rock Mechanics and Engineering.*,
469 34: 480–488, 2015 (in Chinese).

[a18]: Answer to the comment Q7 :

We have revised all references and quotations in the manuscript according to the NHESD journal style. The reference list has been updated as well.

470 Evans, S.G., Tutubalina, O.V., Drobyshev, V.N., Chernomorets, S.S., McDougall, S., Petrakov,
471 D.A., and Hungr, O.: Catastrophic detachment and high-velocity long-runout flow of Kolka
472 Glacier, Caucasus Mountains, Russia in 2002, *Geomorphology.*, 105, 314–321, 2009.

473 Fannin, R.J., and Wise, M.P.: An empirical-statistical model for debris flow travel distance,
474 *Canadian Geotechnical Journal.*, 38, 982–994, 2001.

475 Finlay, P.J., Mostyn, G.R., and Fell, R.: Landslide risk assessment: prediction of travel distance,
476 *Canadian Geotechnical Journal.*, 36, 556–562, 1999.

477 Fell, R., Corominas, J., Bonnard, C., Cascini, L., Leroi, E., and Savage, W. Z.: Guidelines for
478 landslide susceptibility, hazard and risk zoning for land use planning, *Engineering Geology.*,
479 102, 85–98, 2008.

480 Fannin, R., and Wise, M.: An empirical-statistical model for debris flow travel distance, *Can*
481 *Geotech J.*, 38, 982–994, 2001.

482 Glade, T.: Linking debris-flow hazard assessments with geomorphology. *Geomorphology.*, 66(1):
483 189-213, 2005.

484 Glade, T., Anderson, M. G., Crozier, M.J.: *Landslide hazard and risk.* Wiley., 75-138, 2006.

485 GB 50010–2010.: *Code for design concrete structures*, Beijing: Chinese Architectural Industry.,
486 34–80, 2010 (in Chinese).

487 Hebei Province Institute of Hydrogeological and Engineering.: *Geological investigation*
488 *engineering supplemental survey report of Hongse Village Taziping landslide in Hongkou*
489 *Town of Dujiangyan City, Sichuan Province.*, 2010 (in Chinese).

490 Hungr, O.: A Model for the runout analysis of rapid flow slides, debris flows and avalanches, *Can*
491 *Geotech J.*, 32, 610–623, 1995.

492 Hungr, O., Evans, S.G., Bovis, M.J., and Hutchinson, J.N.: A review of the classification of
493 landslides of the flow type, *Environ Eng Geosci.*, 7, 221–238, 2001.

494 Hungr, O., Morgan G.C., and Kellerhals, R.: Quantitative analysis of debris torrent hazards for
495 design of remedial measures, *Can Geotech J.*, 21, 663–677, 1984.

496 Hu, K.H., Cui, P., and Zhang, J.Q., Characteristics of damage to buildings by debris flows on 7
497 August 2010 in Zhouqu, Western China, *Nat Hazards Earth Syst Sci.*, 12, 2209–2217, 2012.

498 Hürlimann, M., Rickenmann, D., Medina, V., and Bateman, A.: Evaluation of approaches to
499 calculate debris-flow parameters for hazard assessment, *Eng Geol.*, 102, 152–163, 2008.

500 Huang, Y., Cheng, H., Dai, Z., Xu, Q., Liu, F., Sawada, K., Moriguchi, S., and Yashima, A.:
501 SPH-based numerical simulation of catastrophic debris flows after the 2008 Wenchuan
502 earthquake, *Bull Eng Geol Environ.*, 74, 1137–1151, 2015.

503 Iverson, R. M., Reid, M. E., and LaHusen, R. G.: Debris-flow mobilization from landslides, *Annu.*
504 *Rev. Earth Planet Sc.*, 25, 85– 138, 1997.

505 Iverson, R.M., and Vallance, J.W.: New views of granular mass flows, *Geology.*, 29, 1115–1118,
506 2001.

507 Iovine, G., Gregorio, S.D., and Lupiano, V.: Debris-flow susceptibility assessment through cellular
508 automata modeling: an example from 15–16 December 1999 disaster at Cervinara and San
509 Martino Valle Caudina (Campania, southern Italy), *Nat Hazards Earth Syst Sci.*, 3, 457–468,
510 2003.

511 Jackson, L.E., Kostashuk, R.A., and MacDonald, G.M.: Identification of debris flow hazard on
512 alluvial fans in the Canadian Rocky mountains, *Geological Society of America.*, 7, 155–124,
513 1987.

514 LeVeque, R.: Finite Volume Methods for Hyperbolic Problems, Cambridge Texts in Applied
515 Mathematics Cambridge University Press., 2002.

~~516 Michael, L.M., 2003. Baynes, F., Scott, G., Granger, K. Regional landslide risk to the Cairns
517 community[J]. Nat Hazards, 2003, 30 (2): 233-249.~~

518 Michael-Leiba, M., Baynes, F., Scott, G., and Granger, K.: Regional landslide risk to the Cairns
519 community, Nat Hazards., 30, 233–249, 2003.

520 Morgenstern, N.R., and Price, V.E.: The analysis of the stability of general slip surfaces,
521 Geotechnique., 15, 79–93, 1965.

~~522 Portilla, M., Chevalier, G., and Hürlimann, M.: Description and analysis of the debris flows
523 occurred during 2008 in the Eastern Pyrenees, Nat. Hazards Earth Syst. Sci., 10, 1635–1645,
524 2010.~~

~~525 Petrazzuoli, S.M., and Zuccaro, G.: Structural resistance of reinforced concrete buildings under
526 pyroclastic flows: a study of the Vesuvian area, J Volcanol Geoth Res., 133, 353–367, 2004.~~

527 Sassa, K., Nagai, S., Solidum, R., Yamazaki, Y., and Ohta, H.: An integrated model simulating the
528 initiation and motion of earthquake and rain induced rapid landslides and its application to
529 the 2006 Leyte landslide, Landslides., 7, 219–236, 2010.

530 Scott, K.M., and Vallance, J.W.: History of Landslides and Debris Flows at Mount Rainier: Water
531 Fact Sheet, USGS Open-File Report., 93–111, 1993.

532 Shi, G.H.: Discontinuous deformation analysis - a new numerical model for the statics and
533 dynamics of block system, Berkeley: University of California., 1988.

~~534 DZ/T 0286-2015.: Specification of risk assessment for geological hazard, Ministry of Land and
535 Resources of the People's Republic of China., 2015 (in Chinese).~~

~~536 Scheidl, C., and Rickenmann, D.: Empirical prediction of debris-flow mobility and deposition on
537 fans, Earth Surf Proc Land., 35, 157–173, 2010.~~

~~538 Toro, E.F.: Riemann problems and the waf method for solving the two dimensional shallow water
539 equations. Philos. Trans. R. Soc. London., Ser. A 338, 43–68, 1992.~~

~~540 Varnes, D.J., : Slope movement types and processes. In: Schuster RL, Krizek RJ (eds) Landslides:
541 analysis and control. Transportation Research Board, National Research Council, Washington,
542 DC, USA., 11–33 , 1978.~~

543 Wang, L., Li, B., Gao, Y., and Zhu, S.: Run-out prediction of large thick-bedded unstable rock: A
544 case study of Daxiang unstable rock in Yangjiao town, Wulong county, Chongqing, Earth
545 Science Frontiers., 23, 251–259, 2016 (in Chinese).

~~546 WSL.: RAMMS: A numerical model for snow avalanches in research and practice, User manual
547 v1.5 avalanche, WSL Institute for snow and avalanche research SLF, Swiss., 2013.~~

~~548 Yin, K.L., Jiang, Q.H., and Wang, Y.: Simulation of Landslide Movement Process by
549 Discontinuous Deformation Analysis, Earth Science Journal of China University of
550 Geosciences, 27, 632–636, 2002 (in Chinese).~~

~~551 Zhang, Y.J.: Study on dynamic characteristics of typical rock avalanche on canyon area, Shanghai
552 Jiao Tong University, 2013 (in Chinese).~~

~~553 Zhang, Z.Y., Wang, S.T., Wang, L.S., Huang, R.Q., Xu, Q., and Tao, L.J.: Principles of
554 engineering geology, Beijing: Geology Press., 212–224, 1993 (in Chinese).~~

555 Zeng, C., Cui, P., Su, Z.M., Lei, Y., Chen, R.: Failure modes of reinforced concrete columns of
556 buildings under debris flow impact, Landslides., 12, 561–571, 2015.